Journal of Materials Chemistry A

HIGHLIGHT

View Article Online
View Journal | View Issue

Cite this: J. Mater. Chem. A, 2018, 6, 21654

Polymeric coatings for applications in electrocatalytic and photoelectrosynthetic fuel production

B. L. Wadsworth, D. Khusnutdinova and G. F. Moore *

Received 18th June 2018
Accepted 1st August 2018

DOI: 10.1039/c8ta05805a

rsc.li/materials-a

Applications of polymeric coatings have emerged as a promising direction for preparing multilayered assemblies and controlling surface properties. In addition to providing a foundation for interfacing soft materials onto solid supports, polymers afford opportunities to develop hybrid constructs with properties difficult to achieve using monolayer-based chemical modification methods. In particular, the microenvironments of polymers are proposed to facilitate charge transfer to redox-active sites, manage delivery of chemical substrates, improve product specificity during catalytic transformations, and lend chemical protection to underpinning solid-state supports as well as embedded components. In this article, we highlight selected examples of polymeric materials utilized in electrocatalytic and photoelectrosynthetic fuel production.

1. Introduction

Human-engineered systems capable of generating fuels from sustainable energy sources provide an approach to satiating modern societies' energy demands, with minimal environmental impact.[1–5] Strategies to address this challenge for science and the imagination[6] often draw inspiration from the biological process of photosynthesis that powers our biosphere and supplied the fossil fuels global economies rely on.[7–11] Catalytic materials directly or indirectly powered by photovoltaics offer pathways to achieving artificial photosynthetic assemblies that store solar energy in the form of chemical bonds, yielding fuels that can be domestically produced and carbon-free or -neutral.[12–21] In this context, the active sites of biological enzymes have inspired researchers to develop molecular complexes that capture key structural and functional principles of nature's catalysts, including their ability to tightly bind substrates, impart alternate reaction coordinate pathways involving relatively low-energy transition states, and weakly bind products.[22–27] However, not all aspects of biological energy transducing systems are or should be targets of chemical mimicry in designing an artificial photosynthesis,[28–30] and some of the more favorable properties associated with solid-state

School of Molecular Sciences, The Biodesign Institute Center for Applied Structural Discovery (CASD), Arizona State University, Tempe, AZ 85287-1604, USA. E-mail: gfmoore@asu.edu

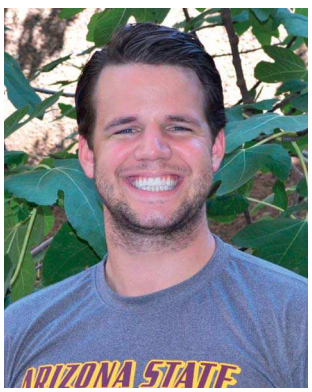

Brian L. Wadsworth is a PhD candidate with Professor Gary F. Moore at Arizona State University and is a National Science Foundation (NSF) Integrative Graduate Education and Research Traineeship (IGERT) fellow. His research includes using electrochemical and spectroscopic techniques to investigate the nano-, micro-, and macro-level properties of molecular fuel-forming electrocatalysts when immobilized at electrified interfaces or dissolved in solution. He received BAs in chemistry and biochemistry from Coe College in Cedar Rapids, Iowa in 2015.

Diana Khusnutdinova received her BS and MS in Chemical Engineering from the Kazan National Research Technological University (2010) and her MS in Nanoscience from Arizona State University (2013). She is currently a Leroy Eyring Fellow and PhD candidate working in the research group of Professor Gary F. Moore in the School of Molecular Sciences at Arizona State University. Her research interests include the design and synthesis of metalloporphyrins and their applications in electrocatalytic and photoelectrosynthetic assemblies for solar energy conversion.

heterogeneous catalysts have motivated several molecular-based, surface-modification strategies.[31–50] The resulting hybrid heterogeneous–homogeneous architectures combine the form factors of their underpinning solid-state supports with molecular coatings allowing synthetic control and tunability of physical properties.

Rationally designed hybrid materials for applications in catalysis have shown enhanced activity, selectivity, lifetime, and recyclability, compared to their constituent parts.[51] However, discovering new and more effective ways to interface the required components and characterize the resulting amalgamation remains challenging.[14] As featured in this article, applications of polymeric coatings, whether covalently tethered to an electrode or deposited as an insoluble film, have emerged as strategies for achieving multilayered molecular functionalization.[32] These approaches involve use of coordination polymers, including: covalent-organic frameworks (COFs), and metal–organic frameworks (MOFs), as well as surface-attached organic polymers, all of which can contain or encapsulate catalytic and/or chromophoric components.

Applications of polymeric materials to immobilize redox-active components at solid-state supports was pioneered by several research groups in the 1970s–1980s, inspiring development of polymer coatings containing catalysts that drive chemical transformations of consequence to renewable energy, at electrified interfaces.[52–74] Reports describing polymer-modified electrode materials include, but are not limited to: coordination of ruthenium to polyvinylpyridine adhered to pyrolytic graphite surfaces,[31] conductivity and electrocatalytic studies of poly-*p*-nitrostyrene-modified electrodes,[52] covalent anchoring of viologen-based polymers to platinum and tin(IV) oxide (SnO_2),[53] polymerization of thin film ruthenium and iron complexes onto various conducting materials,[54] polymerization of pyrrole films containing iron phthalocyanines onto glassy carbon for catalyzing the oxygen reduction reaction,[55] coating of polystyrene on a cadmium sulfide semiconductor for improved water splitting performance,[56] kinetic modeling of electrochemical reactions and their charge transport through surface-bound polymer films,[57] as well as electrooxidation kinetics studies involving a solution dissolved ferrocene analog and a SnO_2 electrode containing croconate violet dyes embedded in a surface-adhered polyvinylpyridine coating.[58]

This article highlights selected examples of more recent advancements in utilizing polymeric materials to prepare hybrid heterogeneous–homogeneous assemblies that drive multielectron, multiproton half-reactions pertinent to renewable energy and solar-fuels generation.[75–102] These chemical transformations include proton, oxygen, and carbon dioxide reduction, as well as water oxidation.

Dr. Gary F. Moore obtained his PhD in Chemistry and Biochemistry at Arizona State University in 2009. In 2011, after completing a Camille and Henry Dreyfus Postdoctoral fellowship at Yale University, he became a staff scientist at Lawrence Berkeley National Laboratory working with the Joint Center for Artificial Photosynthesis (JCAP), a Department of Energy Innovation Hub. In 2014, Moore joined the faculty at Arizona State University as an Assistant Professor in the School of Molecular Sciences. He is a Julie Ann Wrigley Global Institute for Sustainability Scholar, a National Science Foundation (NSF) CAREER Awardee, and in 2017 was recognized by the Achievement Reward for College Scientist (ARCS) Foundation as an outstanding mentor. His research leverages chemical synthesis, surface characterization and electrochemical analysis as tools for improving fundamental understandings of the structure–function relationships governing hard-to-soft matter interfaces.

2. Coordination polymers

Coordination polymers, including COFs and MOFs, have emerged as a class of materials with properties well-suited for functions in electrocatalysis and photoelectrosynthesis. The synthetic versatility of these frameworks facilitates interfacing of structurally well-defined molecular coatings with a variety of electrode materials.[84] In addition to providing a scaffold to incorporate catalytic sites, the ability to chemically alter the framework affords opportunities to control local chemical environments and optimize catalytic performance for driving selected chemical transformations.[103]

COFs typically contain non-metallic building blocks linked together *via* strong, covalent bonds, while MOFs contain metallic clusters or ions connected *via* intervening organic linkers, with both frameworks being ordered, multidimensional structures.[104–107] In general, COFs and MOFs are robust, crystalline structures with permanent porosities and large internal surface areas.[106–110] These features enable substrate diffusion throughout the framework and relatively high loadings of electrochemically active components per unit area.[76,77,107] However, for applications in redox catalysis, a common challenge in working with coordination polymers is facilitating charge transfer to catalytic centers positioned throughout the framework. While some COFs have been reported to achieve relatively high charge-carrier mobilities,[106,111] MOFs are often insulating materials.[76,107] Nonetheless, strategies aimed at increasing electron mobilities have been developed.[112,113] One such approach includes incorporation of conductive guest species,[114,115] but controlling the film thickness and/or positioning of redox sites in pristine MOFs can also alleviate charge transfer issues.[116–120]

2.1 Covalent-organic frameworks

Examples of COF-based electrocatalysts for carbon dioxide (CO_2) reduction incorporating cobalt and copper porphyrin units have been reported by Chang, Yaghi, Yang, and co-workers.[75] These frameworks are constructed *via* imine condensation of 5,10,15,20-tetrakis(4-aminophenyl)porphyrin

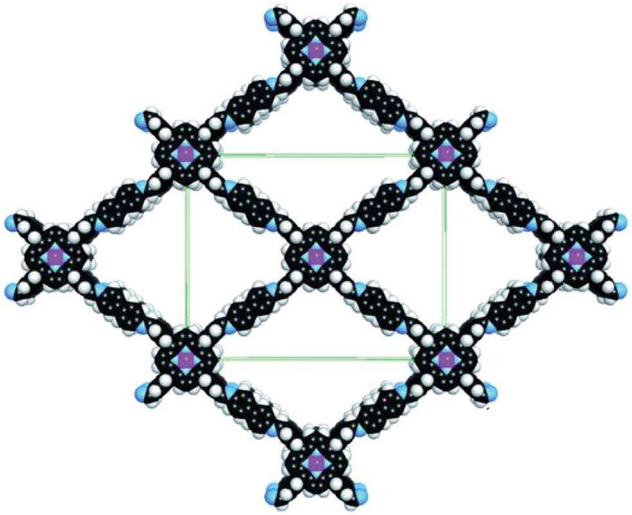

Fig. 1 Space-filling structural model of COF-367-M obtained using Materials Studio 7.0 and refined with experimental powder X-ray diffraction data. From ref. 75. Reprinted with permission from AAAS.

cobalt(II) (CoTAP) and 5,10,15,20-tetrakis(4-aminophenyl) porphyrin copper(II) (CuTAP) with 1,4-benzenedicarboxaldehyde (BDA) or biphenyl-4,4′-dicarboxaldehyde (BPDA) to form COF-366-M and COF-367-M, respectively, where M indicates the presence of metalloporphyrins with varying, yet controllable, ratios of cobalt to copper porphyrin components (Fig. 1). COF-367-M has a larger pore size distribution (12–23 Å), as compared to COF-366-M (10–18 Å), increasing the percentage of redox active cobalt porphyrin sites from 4% to 8% for the all cobalt porphyrin containing samples of COF-366-M and COF-367-M.[75] These particular COFs (COF-366-M and COF-367-M) were targeted to exploit the relatively high charge-carrier mobility of these materials[111] (as compared to other organic crystalline conducting polymers) derived from π-conjugation and π–π stacking interactions.

Electrochemical measurements using samples of COF-366-M or COF-367-M, containing only cobalt porphyrin units and deposited on porous carbon electrodes polarized at −0.67 V *vs.* the reversible hydrogen electrode (RHE) in pH neutral aqueous solutions, indicate the heterogeneous–homogeneous assemblies reduce CO_2 to carbon monoxide (CO) with reported per electroactive cobalt site turnover frequencies (TOFs) of 0.69 and 0.53 s^{-1}, and faradaic efficiencies for CO formation (FE_{CO}) of 90% and 91%, respectively. In these samples, the electroactive cobalt loadings are 1×10^{-8} mol_{Co} cm^{-2} for COF-366-M and 2×10^{-8} mol_{Co} cm^{-2} for COF-367-M. For comparison, control electrochemical experiments performed under the solution and polarization conditions described above, but using electrodes modified with monomeric CoTAP ($\sim 3 \times 10^{-8}$ mol_{Co} cm^{-2}) and no COFs present, yield a per electroactive cobalt site TOF reported at 0.10 s^{-1}. In addition, studies performed under similar solution and polarization conditions using electrodes with deposited samples of COF-367-M containing only 1% cobalt porphyrin and a 99% copper porphyrin balance give a reported per electroactive cobalt site (2×10^{-10} mol_{Co} cm^{-2}) TOF of 2.61 s^{-1}, albeit with a FE_{CO} of 40%.[75]

Characterization using X-ray absorption spectroscopy indicates the electronic structures of the metalloporphyrin components, when incorporated as part of the COF, are modulated in a manner akin to those observed in studies involving homogeneous molecular systems where redox non-innocent ligand behavior is invoked.[75] Thus, the enhancement in catalytic activity of COF-366-M and COF-367-M is in part attributed to altered electronic states of the catalytic metal sites when integrated within the COF structure. This notion is supported by the differences in Tafel slopes measured using electrodes functionalized with the porphyrin-containing COFs (470–550 mV dec^{-1}) *versus* those functionalized with monomeric CoTAP (270 mV dec^{-1}), suggesting the modified electronic states promote access to alternate CO_2 reduction reaction coordinates.[75]

2.2 Metal–organic frameworks

2.2.1 Electrocatalytic metal–organic frameworks. There are several reported examples of MOFs used as catalytic materials.[121–128] This article highlights contributions from the Morris group investigating light-harvesting and electrocatalytic MOF-based architectures.[76–81] In general, synthesis of MOFs with integrated molecular components can be achieved *via* modification of the organic linkers or metal nodes that compose the framework, or *via* post-synthetic introduction of guest species into the MOF pores.

As an example, a MOF capable of catalyzing the oxygen reduction reaction has been formed using Zr_6–oxo clusters as metal nodes and *meso*-tetra(4-carboxyphenyl)porphyrin iron(III) chloride (Fe(III)TCPP) as linker units (Fig. 2).[76] This MOF (PCN-223-Fe) is constructed with zirconium-based nodes that coordinate to carboxyphenyl functional groups of the Fe(III)TCPP macrocycles.[129] Solvothermal synthesis of the PCN-223-Fe MOF on fluorine-doped tin oxide (FTO) yielded electrodes that were analyzed in dimethylformamide (DMF) solutions containing an organic acid proton source. Results from rotating ring-disk

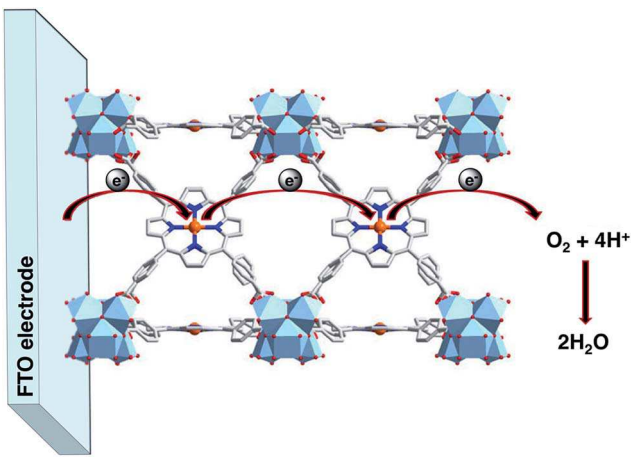

Fig. 2 Schematic depiction showing charge hopping and catalysis using MOF PCN-223-Fe, constructed from Zr_6–oxo clusters and Fe(III) TCPP linker units, on a conductive FTO electrode. Adapted with permission from ref. 76. Copyright 2017, American Chemical Society.

electrode (RRDE) experiments using acetic acid indicate the porphyrin components maintain catalytic activity with high water to hydrogen peroxide (H_2O/H_2O_2) selectivity, achieving a faradaic efficiency of H_2O_2 generation ($FE_{H_2O_2}$) < 6% at potentials < −0.6 V *vs.* the normal hydrogen electrode (NHE).[76] For these assemblies, using a stronger acid as the proton source (trichloroacetic acid in place of acetic acid) results in increased catalytic current densities under the potential range studied, but with poorer product selectivity ($FE_{H_2O_2} \sim 34\%$). The authors mention that further optimization of the MOF, including installment of proton relay pathways near the catalytic centers, could result in improved proton management and product selectivity during catalytic cycling.[76]

Another contribution of Morris and co-workers features incorporation of a molecular ruthenium water-oxidation catalyst, $[Ru(tpy)(dcbpy)OH_2]^{2+}$ (tpy = 2,2′:6′,2″-terpyridine; dcbpy = 5,5-dicarboxy-2,2′-bipyridine), into a Zr-based MOF, UiO-67, forming Ru-UiO-67.[77] The Ru-UiO-67 MOFs are immobilized onto electrode surfaces by placing samples of FTO-coated silicon dioxide into a DMF solution containing $[Ru(tpy)(dcbpy)OH_2]^{2+}$, bi-phenyl-4,4′-dicarboxylic acid (BPDC), and $ZrCl_4$, and heating at 120 °C. In this process, the $[Ru(tpy)(dcbpy)OH_2]^{2+}$ catalysts and BPDC molecules serve as linker molecules, coordinating with Zr^{4+} ions to form $Zr_6O_4(OH)_4(COO)_{12}$ clusters and assemble the MOF. Altering the $[Ru(tpy)(dcbpy)OH_2]^{2+}$/BPDC ratio in the synthesis solution controls the loading of molecular ruthenium catalysts. In general, the reported electroactive ruthenium loadings (3.8×10^{-11} to 1.2×10^{-8} mol_{Ru} cm^{-2}) increase with the total ruthenium loading. For all films studied, the percentage of electroactive ruthenium ranges from 1.4% up to 32.1%.[77] Electrochemical measurements, including RRDE experiments, using the heterogeneous–homogeneous electrodes show the assemblies produce oxygen with a reported per electroactive ruthenium site TOF of 0.2 s^{-1} and faradaic efficiency of 55% when polarized at +1.71 V *vs.* NHE in pH neutral aqueous conditions.[77] These results indicate the hybrid materials retain the catalytic activity of the homogeneous ruthenium catalysts, while bestowing structural properties characteristic of the UiO-67 MOF, thus benefitting from features associated with each of these components.

2.2.2 Photoelectrosynthetic and electrocatalytic metal–organic surfaces. MOFs containing catalytic active sites have also been interfaced with semiconductor surfaces, yielding light-activated heterogeneous–homogeneous materials.[130–132] For example, cobalt dithiolene units have been incorporated into one- and two-dimensional MOFs[82–86] deposited onto glassy carbon (GC) as well as p-type silicon (Si), affording assemblies that under appropriate experimental conditions evolve hydrogen from aqueous solutions. These architectures, prepared by Marinescu and co-workers, are referred to as metal–organic surfaces (MOSs). In particular, one-dimensional cobalt dithiolene coordination polymers, with repeating $[Co(C_6H_2S_4)][Na]$ units (Fig. 3a), have been prepared through liquid–liquid interfacial reactions between cobalt(II) acetate, sodium acetate, and a dinucleating conjugated ligand, benzene-1,2,4,5-tetrathiol (BTT), in the presence of base.[82] Photoelectrochemical measurements using polymeric cobalt BTT

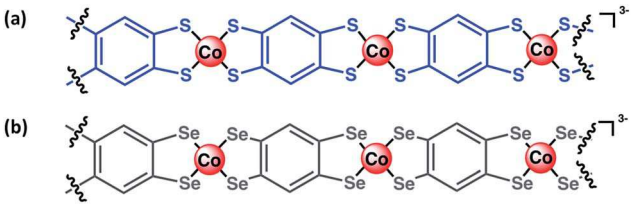

Fig. 3 Structures of cobalt-based coordination polymers based on (a) benzene-1,2,4,5-tetrathiolate and (b) benzene-1,2,4,5-tetraselenolate frameworks. Adapted with permission from ref. 82 and 83. Copyright 2015 and 2017, American Chemical Society.

deposited on Si working electrodes (*p*CoBTT-Si) (total cobalt loading = 4×10^{-6} mol_{Co} cm^{-2}) yield photocurrent densities up to 3.8 mA cm^{-2} when the modified electrodes are polarized at 0 V *vs.* RHE in a pH 1.3 H_2SO_4 aqueous solution under 100 mW cm^{-2} (1-sun) illumination using an air mass 1.5 global (AM1.5G) filter.[82] Additionally, controlled potential electrolysis studies performed under the same solution and illumination conditions indicate *p*CoBTT-Si electrodes generate hydrogen with a faradaic efficiency of 80% when polarized at −0.12 V *vs.* RHE. For comparison, control electrochemical experiments using analogous monomeric cobalt 1,2-benzenedithiolate $[Co(bdt)_2]^-$ units measured in a 1 : 1 mixture of an aqueous pH 1.3 solution in acetonitrile under simulated AM1.5G illumination using a Si working electrode achieve a photocurrent density < 1 mA cm^{-2} when polarized at 0 V *vs.* RHE.[82] Total cobalt loadings on samples of *p*CoBTT-Si were determined from inductively coupled plasma mass spectrometry (ICP-MS) measurements using acid digested samples of MOS coatings that were removed from their Si substrates *via* sonication. The authors also showed that the electroactive cobalt loadings on GC substrates, (5.5×10^{-7} mol_{Co} cm^{-2}) determined using electrochemical methods, coincide with the total cobalt loadings on GC substrates, determined using ICP-MS, indicating a majority of the cobalt centers are electroactive.[82]

Metal dithiolenes incorporated into extended polymer frameworks also display enhanced stability compared to analogous molecular species.[82–85] In accordance with this observation, theoretical studies of homogeneous metal dithiolenes indicate the sulfur moiety of the dithiolene ligand can be protonated during catalytic cycling, resulting in loss of the ligand and decomposition.[83,133–135] Such degradation pathways are minimized in the MOSs, and the dithiolene components, now part of a solid-state assembly, can be utilized in aqueous environments, thus eliminating decomposition processes associated with use of organic solvents.[83]

Inspired by the design and ligand environment of hydrogenase enzymes, Marinescu and co-workers also developed cobalt and nickel selenolate coordination polymers, formed from benzene-1,2,4,5-tetraselenolate (BTSe), as catalysts for the hydrogen evolution reaction (Fig. 3b).[83] In nature, [NiFeSe] hydrogenases, a subclass of [NiFe] hydrogenases containing a selenocysteine residue in place of one of the cysteine residues coordinating the nickel center, demonstrate catalytic activity that is ∼40-fold higher than that achieved by [NiFe]

hydrogenases[136–138] [as measured by the amount of enzyme that produces 1 μmol of H_2 per minute per milligram (U mg^{-1})].[139] It has been proposed that substituting a selenium-moiety for a sulfur-moiety affects the rate of hydrogen desorption from the active site,[140] since selenium–hydrogen bonds (Se–H) are in general weaker than sulfur–hydrogen bonds (S–H). Electrochemical measurements using cobalt BTSe coordination polymers immobilized on a GC working electrode (*p*CoBTSe-GC) indicate the mechanism for hydrogen evolution varies with catalyst loading, a property not observed for the analogous *p*CoBTT-GC constructs.[83] As the measured *p*CoBTSe electroactive cobalt loading increases (3.7×10^{-7} to 9.2×10^{-7} mol_{Co} cm^{-2}), the overpotential required to achieve a current density of 10 mA cm^{-2} decreases from 602–343 mV, with respect to the loadings. The proposed alternative hydrogen evolution reaction (HER) pathway requires interactions between two protonated selenium-moieties, which are more basic than the sulfur-containing assemblies. This step is thus favored only under appropriate catalyst loadings, where the selenium units are in relatively close proximity to each other.[83] Accordingly, *p*CoBTSe-GC (electroactive cobalt loading = 9.2×10^{-7} mol_{Co} cm^{-2}) and *p*CoBTT-GC (electroactive cobalt loading = 5.5×10^{-7} mol_{Co} cm^{-2}) electrodes characterized in pH 1.3 aqueous solutions achieve a current density of 10 mA cm^{-2} at overpotentials of 343 and 560 mV, respectively. The improved catalytic performance for *p*CoBTSe-GC over *p*CoBTT-GC electrodes is attributed in part to their ability to access the proposed alternative reaction mechanism, consistent with the Tafel slopes measured using *p*CoBTSe-GC (97 mV dec^{-1}) and *p*CoBTT-GC (70 mV dec^{-1}) electrodes.[83,86]

3. Surface attached organic polymers and encapsulated molecular components

The assembly of molecular components onto solid-state surfaces using deposited or covalently grafted organic polymers affords another approach to developing hybrid heterogeneous–homogeneous catalysts. In this strategy, the solid surface supports an organic polymeric environment that can house catalytic active sites and/or molecular light absorbing components. The polymeric materials can be post-synthetically modified or already possess appropriate molecular components. Structural features of the polymer can also provide microenvironments that furnish embedded components with properties not associated with their isolated counterparts. When appropriately selected or designed, the polymeric microenvironments aid catalytic performance. The design of such constructs is often inspired by enzymatic proteins, where the assembly of amino acid residues into three-dimensional architectures house an "active site" crucial to facilitating biologically relevant chemical transformations. However, some features associated with enzymes are undesirable for incorporation in technological applications, including their overall poor energy conversion efficiencies, fragility, and relatively large sizes.[23] Borrowing "just the best bits,"[28] it's feasible that constructs integrating favorable attributes of biological assemblies with those of human-engineered materials can be rationally designed and synthesized.[141–143]

3.1 Catalyst-containing organic polymers deposited on conductive substrates

Molecular catalysts encapsulated in polymers, including cobalt porphyrins and phthalocyanines (CoPcs), have been reported to exhibit improved activity and product selectivity.[87,144–148] More specifically, cobalt porphyrins and phthalocyanines when dissolved in solutions or directly immobilized onto conductive surfaces are known to non-selectively catalyze CO_2 and proton reduction.[149–152] However, several groups have shown that when CoPcs are immobilized within a 4-polyvinylpyridine polymer membrane deposited on a carbon-based support, the resulting heterogeneous–homogeneous assembly converts CO_2 to CO with near unity faradaic efficiency.[87,144,145] Herein, we highlight findings from McCrory and co-workers, who developed several hypotheses explaining the enhanced catalytic performance of CoPcs encapsulated within a polymer environment.[87]

The surface functionalization described in their report is achieved by dissolving 4-polyvinylpyridine with CoPcs in solution and drop casting an aliquot onto a pyrolytic graphite electrode surface.[87] The selectivity for CO_2 reduction using this architecture is attributed in part to effects arising from axial coordination of CoPcs to pyridyl units of the polymer. Comparisons of chemically modified carbon electrodes, polarized at −0.73 V *vs.* RHE in a pH 4.7 aqueous solution, containing deposited samples of either CoPcs that are coordinated to a pyridine molecule [CoPc(py)] or CoPcs that are coordinated to the pyridyl units of polyvinylpyridine, yield per cobalt site TOFs that are reported at 1.6 and 4.8 s^{-1}, respectively. Further, these assemblies show a near doubling of the FE_{CO} (68% and 89%, respectively) as compared to that measured in control experiments using electrodes containing deposited CoPcs without pyridine or polymer present (FE_{CO} = 36% and TOF = 0.6 s^{-1}).[87] The total CoPc loadings were constant for each of the samples studied, equalling 1.3×10^{-9} mol_{Co} cm^{-2}. The authors rationalize that axial coordination of CoPcs to pyridyl units raises the energy level of the d_z^2 orbital in the reduced cobalt species (Fig. 4). Thus, upon coordination, the catalyst becomes a stronger nucleophile, facilitating binding and activation of CO_2, and thereby inhibiting proton reduction reaction pathways.[87]

In addition to localized electronic tuning effects, features of the extended polymeric environment have been attributed to augmenting the activity and selectivity of this assembly for CO_2 reduction. For example, in aqueous conditions, some percentage of uncoordinated pyridyl units throughout the polymer network are likely protonated[153,154] and it's proposed that protonated pyridyl units close to the cobalt phthalocyanine–pyridine active sites assist in stabilizing $[CoPc–CO_2]^-$ adducts through hydrogen bonding networks.[87] In addition, the pyridinium species are postulated to serve as local sources of protons, and act as relays that shuttle protons from the bulk solution to CO_2 bound at CoPcs within the polymer.

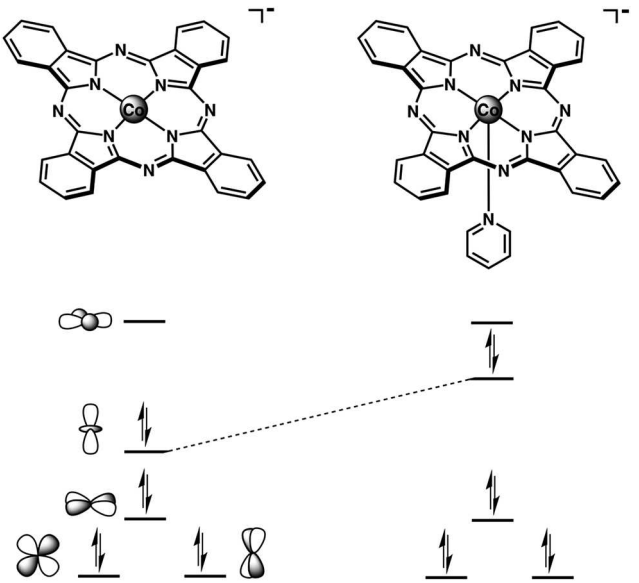

Fig. 4 Relative energies of the cobalt d orbitals in the $1e^-$ reduced forms of CoPc and CoPc(py). As depicted, coordination of CoPc to an axial pyridine raises the energy of the cobalt d_{z^2} orbital. [Ref. 87] – published by the Royal Society of Chemistry.

It can be difficult to separate and study effects that are induced by axial coordination *versus* polymer encapsulation, and the enhanced electrocatalytic properties observed for CoPcs when embedded in a 4-polyvinylpyridine polymer likely result from a combination of complementary processes. Nonetheless, this work features a facile strategy for interfacing molecular electrocatalysts with solid-state materials and indicates an organic polymer can impart unique chemical environments for enhancing catalytic performance.

3.2 Organic polymers containing chromophore–catalyst assemblies

Polymeric materials capable of encapsulating or linking to molecular components have also been utilized in developing dye-sensitized photoelectrosynthetic cells (DSPECs).[88] Meyer and co-workers have shown that polymers can be used (1) strictly as an encapsulating medium, providing protection and stability of embedded dyes and molecular catalysts[89,90] or (2) as a backbone scaffold that can be synthetically manipulated and covalently linked to molecular light-absorbing and/or catalytic components.[91,92]

Chromophores, catalysts, and chromophore–catalyst tandems assembled onto metal-oxide substrates *via* phosphonate linkages often utilize over-layer coatings to avoid desorption under operating conditions.[155–157] Such stabilizing layers are commonly applied using atomic layer deposition (ALD) techniques,[41,158,159] which can require harsh conditions and use of precursors that, upon hydrolysis, result in decomposition of the catalysts and/or dye components.[90] Application of a polymethyl methacrylate (PMMA) encapsulating layer is an alternative approach to protecting phosphonate linkages from hydrolysis. However, oxidation of the surface-bound film by added catalysts can limit the surface stabilization.[89] In contrast to PMMA films, a fluorinated co-polymer (DuPont AF), consisting of 4,5-difluoro-2,2-bis(trifluoromethyl)-1,3-dioxole and tetrafluoro-ethylene, yields an encapsulating layer that remains gas permeable and protects phosphonate linkages to chromophores and catalysts. The coatings are also resistant to high-energy radiation as well as oxidative degradation[90] and have been demonstrated using more than one type of chromophore–catalyst assembly. These results indicate the deposition method is not specific to a particular set of materials or chemical environments and is likely amenable to other molecular assemblies leveraging use of phosphonate linkers on oxide-terminated surfaces.[90]

Meyer and co-workers have also established a novel layer-by-layer method for depositing chromophore–catalyst containing films onto a mesoporous sol–gel SnO_2 thin film containing a titanium(IV) dioxide (TiO_2) over-layer on FTO.[92] The films are formed using poly(acrylic acid) and a polystyrene-based backbone modified with molecular ruthenium water oxidation catalysts (Ru-Cat) as well as ruthenium-based chromophores (Ru-C) (Fig. 5) and the assembly method represents one of few approaches to preparing DSPECs with controllable variation of the dye to catalyst ratios.[160–163] Controlled potential electrolysis measurements using working electrodes prepared from these materials show the assemblies achieve an initial current density

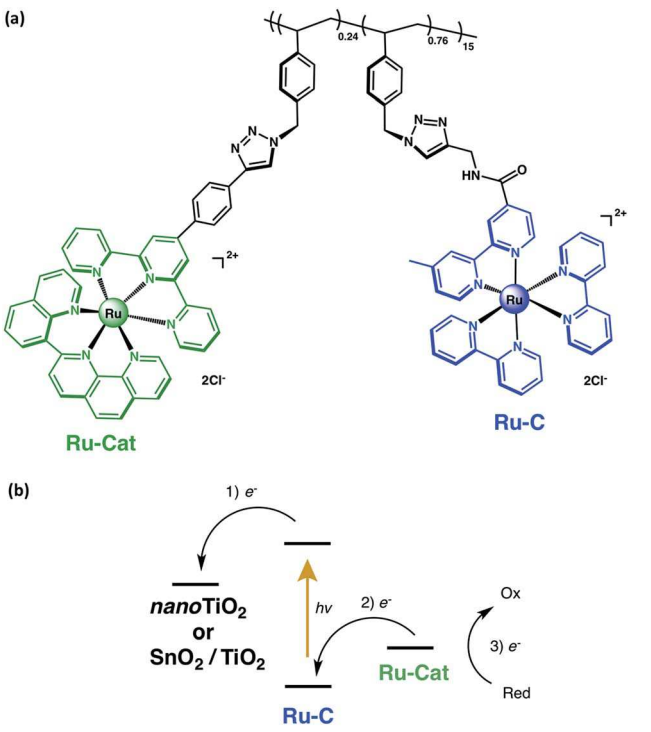

Fig. 5 (a) Chemical structure of a polymeric chromophore–catalyst complex, containing a polystyrene backbone modified with a molecular ruthenium catalyst (Ru-Cat) and chromophore (Ru-C). (b) Schematic depiction showing energetics and sequence of steps for achieving light-activated oxidation using *nano*TiO_2 or SnO_2/TiO_2 electrodes modified with the polymer shown in (a). Adapted with permission from ref. 92. Copyright 2017, American Chemical Society.

of 18.5 μA cm^{-2}, which gradually decreases to 11.5 μA cm^{-2} upon multiple light/dark cycles, when polarized for 140 seconds at +0.2 V *vs.* a silver/silver chloride (Ag/AgCl) electrode in 0.1 M phosphate buffer (pH 7) containing 0.5 M KNO_3 under 1-sun illumination with a 400 nm cutoff filter.[92] Control experiments under the same conditions, but using a chromophore–polymer functionalized electrode containing no Ru-Cat, yield a current density of 7.4 μA cm^{-2} that gradually decreases to 6.2 μA cm^{-2}. The authors attribute the increased photocurrent density of the polymeric catalyst-containing assembly to water oxidation catalyzed by the molecular Ru-Cat.[92] For comparison, 250 second controlled potential electrolysis measurements performed under the conditions previously listed but using a layered electrode assembly, containing a poly ruthenium–chromophore inner layer and molecular ruthenium catalyst-containing outer layer,[91] show electrodes prepared using the polystyrene-based backbone containing both catalyst and light absorber units achieve nearly 30% higher photocurrent densities. The authors ascribe this enhanced performance metric to improved charge transfer dynamics resulting from the spatial positioning of catalysts and light absorbing components in the non-layered, co-functionalized polymer morphology.

3.3 Coordination of molecular catalysts to surface-grafted polymers

Interest in polymer brush materials, polymeric structures grafted to a surface, has motivated approaches for their synthesis, characterization, and application.[163–167] In this section, we highlight efforts from our research group in developing synthetic methodologies to immobilize molecular catalysts onto surface-grafted organic–polymer interfaces.[93–102] The assemblies feature (1) polymeric coatings with appropriate functional groups to direct, template, and assemble molecular catalysts, (2) a protective layer for underpinning surfaces, as well as (3) stabilizing environments for catalysts attached along polymer chains that can be synthetically tailored to control the activity of the overall construct.

The polymer grafting procedure exploits the UV-induced immobilization chemistry of olefins to hydroxyl and oxygen terminated surfaces.[36] In this approach, the surface provides a solid support for synthesizing extended soft environments that house molecular catalysts installed in subsequent wet chemical processing steps. The modularity of this chemistry allows modification of the support material, polymeric interface, or catalysts used in assembling these hybrid architectures, and permits fabrication of electrode assemblies for subsequent electrochemical as well as photoelectrochemical characterization. Publications from our group have demonstrated: (1) these coatings can be prepared on semiconducting as well as conducting substrates,[93–102] (2) the polymer–catalyst grafting is not limited to a specific crystal face orientation,[97] (3) the polymer functional groups can be customized to control the activity of the overall assembly,[98] (4) molecular-level synthetic alterations to the ligand environment of attached molecular catalysts[95,100,101] affect the photoelectrochemical responses observed at the construct level, and (5) the polymer immobilization strategy is not limited to a single class of molecular catalysts.[102]

Achievements using this approach include reporting of 5,10,15,20-tetra-*p*-tolylporphyrin cobalt(II)-polypyridyl thin-film coated gallium phosphide (GaP) photocathodes (Fig. 6a and c) that use solar energy to power hydrogen production from pH neutral aqueous solutions at a rate of ~10 μL min^{-1} cm^{-2}.[102] This rate is obtained under simulated AM1.5G illumination using working electrodes polarized at 0 V *vs.* RHE in a 0.1 M phosphate buffer (pH 7) and equates to a photocurrent density of 1.27 mA cm^2 with a faradaic efficiency of 93%. Given the measured per geometric area total loading of cobalt (0.39×10^{-9} mol_{Co} cm^{-2}), this equates to a HER activity of 18 hydrogen molecules per second per cobalt porphyrin site, a value among the highest reported for a molecular-modified semiconductor operating at the reversible hydrogen electrode potential under simulated AM1.5G illumination. These results confirm that only light, and no electrochemical forward biasing or use of sacrificial redox reagents, supplies the energy input required to generate the fuel. Further, the measured per cobalt porphyrin activity is nearly identical to that achieved using a photoelectrochemical assembly containing directly attached cobalt porphyrins,[100,102] indicating the intervening polymer does not diminish photoelectrosynthetic performance yet reduces the synthetic efforts required to immobilize the porphyrin units.

Structural characterization of these samples includes use of surface sensitive X-ray-based techniques, grazing angle attenuated total reflectance Fourier transform infrared spectroscopy, ellipsometry, and ICP-MS, performed prior to and following photoelectrochemical studies. In addition to confirming the cobalt macrocycles remain intact and are indeed coordinated to pyridyl nitrogen sites along the polymer graft, these complimentary techniques yield quantitative information on the per geometric area cobalt porphyrin surface concentration and fraction of pyridyl sites coordinated to a cobalt porphyrin center. Further, these characterization methods are not limited to analysis of cobalt porphyrin–polypyridyl coated GaP samples and have been applied to constructs containing cobaloxime or difluoroborylcobaloxime type catalysts[93–96,99] as well as assemblies constructed using polyvinylimidazole brushes.[97,98]

In addition to modification of semiconducting surfaces, we have reported the use of transparent conductive oxide (TCO) substrates to prepare polymeric catalysts containing assemblies for electrocatalytic applications.[99] In an example using a cobaloxime–polypyridyl coated electrode composed from nanostructured indium tin oxide (ITO) (Fig. 6b and d), we have shown: (1) electrochemical and spectroscopic evidence that a polypyridyl–cobaloxime attachment chemistry initially developed for use on semiconductor surfaces can also be used to functionalize TCO substrates, (2) direct electrochemical measurements of redox features assigned to polymer-immobilized catalysts at potentials that are insulating using semiconducting substrates, (3) comparisons of the catalyst–polymer redox features observed in organic *versus* aqueous solvents, (4) a comparison of the electrochemically active cobaloxime loading *versus* total cobalt loading on the polymer, (5) the difference in applied potentials required to achieve

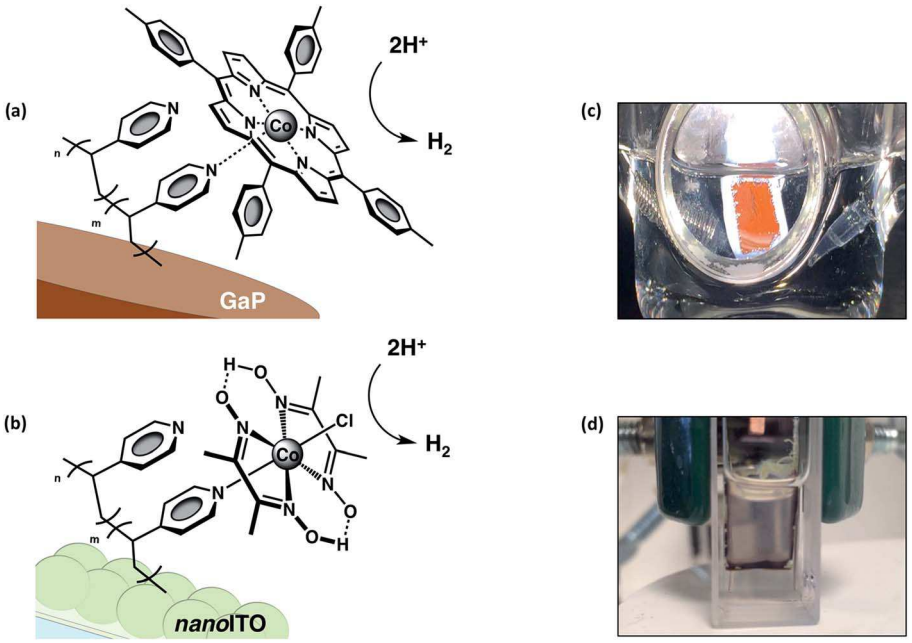

Fig. 6 Schematic depictions of (a) a cobalt porphyrin immobilized onto a gallium phosphide semiconductor *via* coordination to a surface-grafted polyvinylpyridine chain and (b) a cobaloxime immobilized onto a nanostructured indium tin oxide electrode *via* coordination to a surface-grafted polyvinylpyridine chain. Images of (c) a cobalt porphyrin–polypyridyl coated electrode under 100 mW cm^{-2} simulated solar illumination in a neutral aqueous 0.1 M phosphate buffer solution and (d) a cobaloxime–polypyridyl coated electrode polarized in a 0.1 M tetrabutylammonium perchlorate/propylene carbonate solution at a potential required to generate reduced Co(I) species within the surface-grafted polymer. Adapted with permission from ref. 99 and 102. Copyright 2016 and 2017, American Chemical Society.

a similar per cobalt hydrogen production activity when using the cobaloxime–polypyridine-*nano*ITO cathode *versus* a cobaloxime–polypyridine-GaP photocathode is approximately equal to the open circuit voltage of the semiconductor assembly, (6) direct spectroscopic evidence of reduced catalysts within the confines of the surface-grafted polymer, and (7) potential extension of cobaloxime–polymer constructs to photovoltaic-electrolysis approaches for producing solar fuels.

Electrochemical studies using these polypyridyl–cobaloxime modified ITO electrodes in an organic electrolyte solution (0.1 M tetrabutylammonium perchlorate in propylene carbonate) show ~20% of the cobalt centers within these films are electroactive under these conditions (total cobalt loading = 31×10^{-9} mol_{Co} cm^{-2}; electroactive cobalt loading = 6×10^{-9} mol_{Co} cm^{-2}). These results suggest exploration of alternative polymeric architectures, solvation environments, or design of scaffolds with embedded redox mediators could increase the percentage of electroactive metal centers in surface-grafted polymeric assemblies, resulting in further catalytic activity gains.

4. Conclusions and outlook

Managing interfacial chemistry using polymeric coatings offers new opportunities to control matter and energy at the nano-, meso-, and macro-scales. The strategies highlighted in this article feature the ability to chemically tailor materials for driving chemical transformations that address energy needs and societal demands. While structurally more complex than their components, these hierarchical materials move beyond the use of traditional model systems and towards studying the basic energy science of catalysis in chemical environments approaching complexities encountered in real-world applications. Despite the promise of these approaches, finding new and more effective ways to interface soft materials onto electrode surfaces and characterize the resulting hybrid materials remains a challenge, requiring discoveries and innovations in the areas of surface chemistry, electrocatalysis, and photoelectrochemical energy transduction. We imagine advances in physical measurement capabilities coupled with progress in computational and theoretical modeling will continue to provide improved understandings of the structure–function relationships governing these assemblies, further accelerating synthetic efforts aimed at improving their electrocatalytic and photoelectrosynthetic performance.

Conflicts of interest

There are no conflicts to declare.

Acknowledgements

This material is based upon work supported by the National Science Foundation under Early Career Award 1653982. B. L. W. was supported by an IGERT-SUN fellowship funded by the National Science Foundation (1144616).

Notes and references

1 T. A. Faunce, W. Lubitz, A. W. Rutherford, D. MacFarlane, G. F. Moore, P. Yang, D. G. Nocera, T. A. Moore, D. H. Gregory, S. Fukuzumi, K. B. Yoon, F. A. Armstrong, M. R. Wasielewski and S. Styring, *Energy Environ. Sci.*, 2013, **6**, 695–698.

2 T. A. Faunce, S. Styring, M. R. Wasielewski, G. W. Brudvig, A. W. Rutherford, J. Messinger, A. F. Lee, C. L. Hill, H. DeGroot, M. Fontecave, D. R. MacFarlane, B. Hankamer, D. G. Nocera, D. M. Tiede, H. Dau, W. Hillier, L. Wang and R. Amal, *Energy Environ. Sci.*, 2013, **6**, 1074–1076.

3 M. Hambourger, G. F. Moore, D. M. Kramer, D. Gust, A. L. Moore and T. A. Moore, *Chem. Soc. Rev.*, 2009, **38**, 25–35.

4 N. S. Lewis, *Science*, 2016, **351**, aad1920.

5 D. G. Nocera, *Acc. Chem. Res.*, 2017, **50**, 616–619.

6 *Directing Matter and Energy: Five Challenges for Science and the Imagination*, U.S. Department of Energy: Basic Energy Sciences Advisory Committee (BESAC) Report, U.S. Government Printing Office, Washington, DC, 2007.

7 R. E. Blankenship, D. M. Tiede, J. Barber, G. W. Brudvig, G. Fleming, M. Ghirardi, M. R. Gunner, W. Junge, D. M. Kramer, A. Melis and T. A. Moore, *Science*, 2011, **332**, 805–809.

8 D. R. Ort, S. S. Merchant, J. Alric, A. Barkan, R. E. Blankenship, R. Bock, R. Croce, M. R. Hanson, J. M. Hibberd, S. P. Long and T. A. Moore, *Proc. Natl. Acad. Sci. U. S. A.*, 2015, **112**, 8529–8536.

9 J. Barber and P. D. Tran, *J. R. Soc., Interface*, 2013, **10**, 20120984.

10 J. R. Schramski, D. K. Gattie and J. H. Brown, *Proc. Natl. Acad. Sci. U. S. A.*, 2015, **112**, 9511–9517.

11 V. Smil, *Popul. Dev. Rev.*, 2011, **37**, 613–636.

12 T. W. Woolerton, S. Sheard, Y. S. Chaudhary and F. A. Armstrong, *Energy Environ. Sci.*, 2012, **5**, 7470–7490.

13 M. G. Walter, E. L. Warren, J. R. McKone, S. W. Boettcher, Q. Mi, E. A. Santori and N. S. Lewis, *Chem. Rev.*, 2010, **110**, 6446–6473.

14 J. R. McKone, S. C. Marinescu, B. S. Brunschwig, J. R. Winkler and H. B. Gray, *Chem. Sci.*, 2014, **5**, 865–878.

15 A. J. Nozik, *Annu. Rev. Phys. Chem.*, 1978, **29**, 189–222.

16 A. J. Bard and M. A. Fox, *Acc. Chem. Res.*, 1995, **28**, 141–145.

17 D. Gust, T. A. Moore and A. L. Moore, *Acc. Chem. Res.*, 2009, **42**, 1890–1898.

18 G. F. Moore and G. W. Brudvig, *Annu. Rev. Condens. Matter Phys.*, 2011, **2**, 303–327.

19 Y. Tachibana, L. Vayssieres and J. R. Durrant, *Nat. Photonics*, 2012, **6**, 511.

20 B. Kumar, M. Llorente, J. Froehlich, T. Dang, A. Sathrum and C. P. Kubiak, *Annu. Rev. Phys. Chem.*, 2012, **63**, 541–569.

21 S. Ardo, D. F. Rivas, M. A. Modestino, V. S. Greiving, F. F. Abdi, E. A. Llado, V. Artero, K. Ayers, C. Battaglia, J. P. Becker, D. Bederak, A. Berger, F. Buda, E. Chinello, B. Dam, V. Di Palma, T. Edvinsson, K. Fujii, H. Gardeniers, H. Geerlings, S. M. H. Hashemi, S. Haussener, F. Houle, J. Huskens, B. D. James, K. Konrad, A. Kudo, P. P. Kunturu, D. Lohse, B. Mei, E. L. Miller, G. F. Moore, J. Muller, K. L. Orchard, T. E. Rosser, F. H. Saadi, J. W. Schüttauf, B. Seger, S. W. Sheehan, W. A. Smith, J. Spurgeon, M. H. Tang, R. van de Krol, P. C. K. Vesborg and P. Westerik, *Energy Environ. Sci.*, 2018, DOI: 10.1039/C7EE03639F.

22 J. A. Cracknell, K. A. Vincent and F. A. Armstrong, *Chem. Rev.*, 2008, **108**, 2439–2461.

23 F. A. Armstrong and J. Hirst, *Proc. Natl. Acad. Sci. U. S. A.*, 2011, **108**, 14049–14054.

24 M. Rakowski DuBois and D. L. DuBois, *Chem. Soc. Rev.*, 2009, **38**, 62–72.

25 M. L. Helm, M. P. Stewart, R. M. Bullock, M. Rakowski DuBois and D. L. DuBois, *Science*, 2011, **333**, 863–866.

26 M. Bacchi, G. Berggren, J. Niklas, E. Veinberg, M. W. Mara, M. L. Shelby, O. G. Poluektov, L. X. Chen, D. M. Tiede, C. Cavazza, M. J. Field, M. Fontecave and V. Artero, *Inorg. Chem.*, 2014, **53**, 8071–8082.

27 B. Ginovska-Pangovska, A. Dutta, M. L. Reback, J. C. Linehan and W. J. Shaw, *Acc. Chem. Res.*, 2014, **47**, 2621–2630.

28 A. W. Rutherford and T. A. Moore, *Nature*, 2008, **453**, 449–450.

29 G. D. Scholes, G. R. Fleming, A. Olaya-Castro and R. Van Grondelle, *Nat. Chem.*, 2011, **3**, 763.

30 F. E. Osterloh, *ACS Energy Lett.*, 2017, **2**, 445–453.

31 N. Oyama and F. C. Anson, *J. Am. Chem. Soc.*, 1979, **101**, 3450–3456.

32 R. W. Murray, *Philos. Trans. R. Soc. London, Ser. A*, 1981, **302**, 253–265.

33 M. S. Wrighton, *Science*, 1986, **231**, 32–37.

34 M. D. Porter, T. B. Bright, D. L. Allara and C. E. Chidsey, *J. Am. Chem. Soc.*, 1987, **109**, 3559–3568.

35 A. Le Goff, V. Artero, B. Jousselme, P. D. Tran, N. Guillet, R. Métayé, A. Fihri, S. Palacin and M. Fontecave, *Science*, 2009, **326**, 1384–1387.

36 X. Wang, R. E. Ruther, J. A. Streifer and R. J. Hamers, *J. Am. Chem. Soc.*, 2010, **132**, 4048–4049.

37 E. S. Andreiadis, P. A. Jacques, P. D. Tran, A. Leyris, M. Chavarot-Kerlidou, B. Jousselme, M. Matheron, J. Pécaut, S. Palacin, M. Fontecave and V. Artero, *Nat. Chem.*, 2013, **5**, 48–53.

38 M. Ugeda, A. J. Bradley, L. Rodrigo, M. Yu, W. Liu, P. Doak, A. Riss, J. B. Neaton, T. D. Tilley, R. Pérez and M. F. Crommie, *J. Phys. Chem. C*, 2016, **120**, 26448–26452.

39 S. Oh, J. R. Gallagher, J. T. Miller and Y. Surendranath, *J. Am. Chem. Soc.*, 2016, **138**, 1820–1823.

40 J. J. Leung, J. Warnan, D. H. Nam, J. Z. Zhang, J. Willkomm and E. Reisner, *Chem. Sci.*, 2017, **8**, 5172–5180.

41 J. Gu, Y. Yan, J. L. Young, K. X. Steirer, N. R. Neale and J. A. Turner, *Nat. Mater.*, 2015, **15**, 456.

42 S. J. Wilkins, T. Paskova, C. L. Reynolds and A. Ivanisevic, *ChemPhysChem*, 2015, **16**, 1687–1694.

43 A. M. Carey, H. Zhang, D. Mieritz, A. Volosin, A. T. Gardiner, R. J. Cogdell, H. Yan, D. K. Seo, S. Lin and N. W. Woodbury, *ACS Appl. Mater. Interfaces*, 2016, **8**, 25104–25110.
44 J. Seo, R. T. Pekarek and M. J. Rose, *Chem. Commun.*, 2015, **51**, 13264–13267.
45 J. R. C. Lattimer, J. D. Blakemore, W. Sattler, S. Gul, R. Chatterjee, V. K. Yachandra, J. Yano, B. S. Brunschwig, N. S. Lewis and H. B. Gray, *Dalton Trans.*, 2014, **43**, 15004–15012.
46 B. Reuillard, K. H. Ly, T. E. Rosser, M. F. Kuehnel, I. Zebger and E. Reisner, *J. Am. Chem. Soc.*, 2017, **139**, 14425–14435.
47 J. J. Concepcion, J. W. Jurss, M. K. Brennaman, P. G. Hoertz, A. O. T. Patrocinio, N. Y. Murakami Iha, J. L. Templeton and T. J. Meyer, *Acc. Chem. Res.*, 2009, **42**, 1954–1965.
48 Y. Sun, J. Sun, J. R. Long, P. Yang and C. J. Chang, *Chem. Sci.*, 2013, **4**, 118–124.
49 J. Mukherjee, S. Peczonczyk and S. Maldonado, *Langmuir*, 2010, **26**, 10890–10896.
50 Y. Hou, B. L. Abrams, P. C. K. Vesborg, M. E. Björketun, K. Herbst, L. Bech, A. M. Setti, C. D. Damsgaard, T. Pedersen, O. Hansen, J. Rossmeisl, S. Dahl, J. K. Nørskov and I. Chorkendorff, *Nat. Mater.*, 2011, **10**, 434–438.
51 R. Ye, J. Zhao, B. B. Wickemeyer, F. D. Toste and G. A. Somorjai, *Nat. Catal.*, 2018, **1**, 318–325.
52 M. R. Van de Mark and L. L. Miller, *J. Am. Chem. Soc.*, 1978, **100**, 3223–3225.
53 D. C. Bookbinder and M. S. Wrighton, *J. Electrochem. Soc.*, 1983, **130**, 1080–1087.
54 H. D. Abruña, P. Denisevich, M. Umana, T. J. Meyer and R. W. Murray, *J. Am. Chem. Soc.*, 1981, **103**, 1–5.
55 R. A. Bull, F. R. Fan and A. J. Bard, *J. Electrochem. Soc.*, 1984, **131**, 687–689.
56 A. J. Frank and K. Honda, *J. Photochem.*, 1985, **29**, 195–204.
57 C. P. Andrieux and J. M. Saveant, *J. Electroanal. Chem. Interfacial Electrochem.*, 1978, **93**, 163–168.
58 P. V. Kamat and M. A. Fox, *J. Electroanal. Chem. Interfacial Electrochem.*, 1983, **159**, 49–62.
59 R. W. Murray, *Acc. Chem. Res.*, 1980, **13**, 135–141.
60 T. Ikeda, C. R. Leidner and R. W. Murray, *J. Electroanal. Chem. Interfacial Electrochem.*, 1982, **138**, 343–365.
61 R. W. Murray, *Annu. Rev. Mater. Sci.*, 1984, **14**, 145–169.
62 R. W. Murray, A. G. Ewing and R. A. Durst, *Anal. Chem.*, 1987, **59**, 379A–390A.
63 T. R. O'Toole, B. P. Sullivan, M. R. M. Bruce, L. D. Margerum, R. W. Murray and T. J. Meyer, *J. Electroanal. Chem. Interfacial Electrochem.*, 1989, **259**, 217–239.
64 N. Oyama and F. C. Anson, *Anal. Chem.*, 1980, **52**, 1192–1198.
65 A. Deronzier and J. C. Moutet, *Acc. Chem. Res.*, 1989, **22**, 249–255.
66 B. I. Podlovchenko and V. N. Andreev, Electrocatalysis on polymer-modified electrodes, *Russ. Chem. Rev.*, 2002, **71**, 837–851.
67 E. Puodziukynaite, L. Wang, K. S. Schanze, J. M. Papanikolas and J. R. Reynolds, *Polym. Chem.*, 2014, **5**, 2363.
68 L. Wang, E. Puodziukynaite, R. P. Vary, E. M. Grumstrup, R. M. Walczak, O. Y. Zolotarskaya, K. S. Schanze, J. R. Reynolds and J. M. Papanikolas, *J. Phys. Chem. Lett.*, 2012, **3**, 2453.
69 P. D. Tran, T. V. Tran, M. Orio, S. Torelli, Q. D. Truong, K. Nayuki, Y. Sasaki, S. Y. Chiam, R. Yi, I. Honma and J. Barber, *Nat. Mater.*, 2016, **15**, 640.
70 S. Ponnurangam, I. V. Chernyshova and P. Somasundaran, *Adv. Colloid Interface Sci.*, 2017, **244**, 184–198.
71 A. A. Oughli, A. Ruff, N. P. Boralugodage, P. Rodríguez-Maciá, N. Plumeré, W. Lubitz, W. J. Shaw, W. Schuhmann and O. Rüdiger, *Nat. Commun.*, 2018, **9**, 864.
72 Z. Kap, E. Ülker, S. V. K. Nune and F. Karadas, *J. Appl. Electrochem.*, 2018, **48**, 201–209.
73 N. U. Day, C. C. Wamser and M. G. Walter, *Polym. Int.*, 2015, **64**, 833–857.
74 C. S. Diercks, S. Lin, N. Kornienko, E. A. Kapustin, E. M. Nichols, C. Zhu, Y. Zhao, C. J. Chang and O. M. Yaghi, *J. Am. Chem. Soc.*, 2018, **140**, 1116–1122.
75 S. Lin, C. S. Diercks, Y. B. Zhang, N. Kornienko, E. M. Nichols, Y. Zhao, A. R. Paris, D. Kim, P. Yang, O. M. Yaghi and C. J. Chang, *Science*, 2015, **349**, 1208–1213.
76 P. M. Usov, B. Huffman, C. C. Epley, M. C. Kessinger, J. Zhu, W. A. Maza and A. J. Morris, *ACS Appl. Mater. Interfaces*, 2017, **9**, 33539–33543. Link: https://pubs.acs.org/doi/abs/10.1021/acsami.7b01547. Note: Further permissions related to the material excerpted should be directed to the American Chemical Society.
77 S. Lin, Y. Pineda-Galvan, W. A. Maza, C. C. Epley, J. Zhu, M. C. Kessinger, Y. Pushkar and A. J. Morris, *ChemSusChem*, 2017, **10**, 514–522.
78 P. M. Usov, S. R. Ahrenholtz, W. A. Maza, B. Stratakes, C. C. Epley, M. C. Kessinger, J. Zhu and A. J. Morris, *J. Mater. Chem. A*, 2016, **4**, 16818–16823.
79 S. Lin, A. K. Ravari, J. Zhu, P. M. Usov, M. Cai, S. R. Ahrenholtz, Y. Pushkar and A. J. Morris, *ChemSusChem*, 2018, **11**, 464–471.
80 W. A. Maza, A. J. Haring, S. R. Ahrenholtz, C. C. Epley, S. Y. Lin and A. J. Morris, *Chem. Sci.*, 2016, **7**, 719–727.
81 J. Zhu, W. A. Maza and A. J. Morris, *J. Photochem. Photobiol., A*, 2017, **344**, 64–77.
82 C. A. Downes and S. C. Marinescu, *J. Am. Chem. Soc.*, 2015, **137**, 13740–13743.
83 C. A. Downes and S. C. Marinescu, *ACS Catal.*, 2016, **7**, 848–854.
84 A. J. Clough, J. W. Yoo, M. H. Mecklenburg and S. C. Marinescu, *J. Am. Chem. Soc.*, 2015, **137**, 118–121.
85 C. A. Downes and S. C. Marinescu, *Dalton Trans.*, 2016, **45**, 19311–19321.
86 C. A. Downes, J. W. Yoo, N. M. Orchanian, R. Haiges and S. C. Marinescu, *Chem. Commun.*, 2017, **53**, 7306–7309.
87 W. W. Kramer and C. C. L. McCrory, *Chem. Sci.*, 2016, **7**, 2506–2515.

88 D. L. Ashford, M. K. Gish, A. K. Vannucci, M. K. Brennaman, J. L. Templeton, J. M. Papanikolas and T. J. Meyer, *Chem. Rev.*, 2015, **115**, 13006–13049.
89 K. R. Wee, M. K. Brennaman, L. Alibabaei, B. H. Farnum, B. Sherman, A. M. Lapides and T. J. Meyer, *J. Am. Chem. Soc.*, 2014, **136**, 13514–13517.
90 M. S. Eberhart, K. R. Wee, S. Marquard, K. Skinner, D. Wang, A. Nayak and T. J. Meyer, *ChemSusChem*, 2017, **10**, 2380–2384.
91 G. Leem, Z. A. Morseth, K. R. Wee, J. Jiang, M. K. Brennaman, J. M. Papanikolas and K. S. Schanze, *Chem.–Asian J.*, 2016, **11**, 1257–1267.
92 J. Jiang, B. D. Sherman, Y. Zhao, R. He, I. Ghiviriga, L. Alibabaei, T. J. Meyer, G. Leem and K. S. Schanze, *ACS Appl. Mater. Interfaces*, 2017, **9**, 19529–19534.
93 A. Krawicz, J. Yang, E. Anzenberg, J. Yano, I. D. Sharp and G. F. Moore, *J. Am. Chem. Soc.*, 2013, **135**, 11861–11868.
94 A. Krawicz, D. Cedeno and G. F. Moore, *Phys. Chem. Chem. Phys.*, 2014, **16**, 15818–15824.
95 D. Cedeno, A. Krawicz, P. Doak, M. Yu, J. B. Neaton and G. F. Moore, *J. Phys. Chem. Lett.*, 2014, **5**, 3222–3226.
96 D. Cedeno, A. Krawicz and G. F. Moore, *Interface Focus*, 2015, **5**, 20140085.
97 A. M. Beiler, D. Khusnutdinova, S. I. Jacob and G. F. Moore, *ACS Appl. Mater. Interfaces*, 2016, **8**, 10038–10047.
98 A. M. Beiler, D. Khusnutdinova, S. I. Jacob and G. F. Moore, *Ind. Eng. Chem. Res.*, 2016, **55**, 5306–5314.
99 B. L. Wadsworth, A. M. Beiler, D. Khusnutdinova, S. I. Jacob and G. F. Moore, *ACS Catal.*, 2016, **6**, 8048–8057.
100 D. Khusnutdinova, A. M. Beiler, B. L. Wadsworth, S. I. Jacob and G. F. Moore, *Chem. Sci.*, 2017, **8**, 253–259.
101 D. Khusnutdinova, M. Flores, A. M. Beiler and G. F. Moore, *Photosynthetica*, 2018, **56**, 67–74.
102 A. M. Beiler, D. Khusnutdinova, B. L. Wadsworth and G. F. Moore, *Inorg. Chem.*, 2017, **56**, 12178–12185.
103 H. Furukawa, K. E. Cordova, M. O'Keeffe and O. M. Yaghi, *Science*, 2013, **341**, 1230444.
104 O. M. Yaghi, M. O'keeffe, N. W. Ockwig, H. K. Chae, M. Eddaoudi and J. Kim, *Nature*, 2003, **423**, 705–714.
105 X. Feng, X. Ding and D. Jiang, *Chem. Soc. Rev.*, 2012, **41**, 6010–6022.
106 C. S. Diercks and O. M. Yaghi, *Science*, 2017, **355**, eaal1585.
107 C. A. Downes and S. C. Marinescu, *ChemSusChem*, 2017, **10**, 4374–4392.
108 V. S. Vyas, F. Haase, L. Stegbauer, G. Savasci, F. Podjaski, C. Ochsenfeld and B. V. Lotsch, *Nat. Commun.*, 2015, **6**, 8508.
109 B. C. Patra, S. Khilari, R. N. Manna, S. Mondal, D. Pradhan, A. Pradhan and A. Bhaumik, *ACS Catal.*, 2017, **7**, 6120–6127.
110 T. Banerjee, K. Gottschling, G. Savaci, C. Ochsenfeld and B. V. Lotsch, *ACS Energy Lett.*, 2018, **3**, 400–409.
111 S. Wan, F. Gándara, A. Asano, H. Furukawa, A. Saeki, S. K. Dey, L. Liao, M. W. Ambrogio, Y. Y. Botros, X. Duan and S. Seki, *Chem. Mater.*, 2011, **23**, 4094–4097.
112 L. Sun, M. G. Campbell and M. Dinca, *Angew. Chem., Int. Ed.*, 2016, **55**, 3566–3579.
113 D. M. D'Alessandro, J. R. Kanga and J. S. Caddy, *Aust. J. Chem.*, 2011, **64**, 718–722.
114 C. W. Kung, J. E. Mondloch, T. C. Wang, W. Bury, W. Hoffeditz, B. M. Klahr, R. C. Klet, M. J. Pellin, O. K. Farha and J. T. Hupp, *ACS Appl. Mater. Interfaces*, 2015, **7**, 28223–28230.
115 I. Hod, P. Deria, W. Bury, J. E. Mondloch, C. W. Kung, M. So, M. D. Sampson, A. W. Peters, C. P. Kubiak, O. K. Farha and J. T. Hupp, *Nat. Commun.*, 2015, **6**, 8304.
116 J. Liu and C. Wöll, *Chem. Soc. Rev.*, 2017, **46**, 5730–5770.
117 S. R. Ahrenholtz, C. C. Epley and A. J. Morris, *J. Am. Chem. Soc.*, 2014, **136**, 2464–2472.
118 A. J. Clough, J. M. Skelton, C. A. Downes, A. A. De La Rosa, J. W. Yoo, A. Walsh, B. C. Melot and S. C. Marinescu, *J. Am. Chem. Soc.*, 2017, **139**, 10863–10867.
119 C. A. Downes and S. C. Marinescu, *ACS Catal.*, 2017, **7**, 8605–8612.
120 S. Lin, P. M. Usov and A. J. Morris, *Chem. Commun.*, 2018, **54**, 6965–6974.
121 S. Roy, V. Pascanu, S. Pullen, G. González Miera, B. Martín-Matute and S. Ott, *Chem. Commun.*, 2017, **53**, 3257–3260.
122 B. A. Johnson, A. Bhunia and S. Ott, *Dalton Trans.*, 2017, **46**, 1382–1388.
123 S. Roy, A. Bhunia, N. Schuth, M. Haumann and S. Ott, *Sustainable Energy Fuels*, 2018, **2**, 1148–1152.
124 L. Ye, J. Liu, Y. Gao, C. Gong, M. Addicoat, T. Heine, C. Wöll and L. Sun, *J. Mater. Chem. A*, 2016, **4**, 15320–15326.
125 I. Hod, M. D. Sampson, P. Deria, C. P. Kubiak, O. K. Farha and J. T. Hupp, *ACS Catal.*, 2015, **5**, 6302–6309.
126 N. Kornienko, Y. Zhao, C. S. Kley, C. Zhu, D. Kim, S. Lin, C. J. Chang, O. M. Yaghi and P. Yang, *J. Am. Chem. Soc.*, 2015, **137**, 14129–14135.
127 C. Wang, Z. Xie, K. E. deKrafft and W. Lin, *J. Am. Chem. Soc.*, 2011, **133**, 13445–13454.
128 M. Lions, J. B. Tommasino, R. Chattot, B. Abeykoon, N. Guillou, T. Devic, A. Demessence, L. Cardenas, F. Maillard and A. Fateeva, *Chem. Commun.*, 2017, **53**, 6496–6499.
129 D. Feng, Z. Y. Gu, Y. P. Chen, J. Park, Z. Wei, Y. Sun, M. Bosch, S. Yuan and H. C. Zhou, *J. Am. Chem. Soc.*, 2014, **136**, 17714–17717.
130 J. He, Z. Yan, J. Wang, J. Xie, L. Jiang, Y. Shi, F. Yuan, F. Yu and Y. Sun, *Chem. Commun.*, 2013, **49**, 6761–6763.
131 R. Lin, L. Shen, Z. Ren, W. Wu, Y. Tan, H. Fu, J. Zhang and L. Wu, *Chem. Commun.*, 2014, **50**, 8533–8535.
132 S. Pullen and S. Ott, *Top. Catal.*, 2016, **59**, 1712–1721.
133 W. T. Eckenhoff, W. R. McNamara, P. Du and R. Eisenberg, *Biochim. Biophys. Acta, Bioenerg.*, 2013, **1827**, 958–973.
134 B. H. Solis and S. Hammes-Schiffer, *J. Am. Chem. Soc.*, 2012, **134**, 15253–15256.
135 C. S. Letko, J. A. Panetier, M. Head-Gordon and T. D. Tilley, *J. Am. Chem. Soc.*, 2014, **136**, 9364–9376.
136 E. Garcin, X. Vernede, E. C. Hatchikian, A. Volbeda, M. Frey and J. C. Fontecilla-Camps, *Structure*, 1999, **7**, 557–566.
137 A. Parkin, G. Goldet, C. Cavazza, J. C. Fontecilla-Camps and F. A. Armstrong, *J. Am. Chem. Soc.*, 2008, **130**, 13410–13416.

138 C. Wombwell, C. A. Caputo and E. Reisner, *Acc. Chem. Res.*, 2015, **48**, 2858–2865.
139 F. M. Valente, A. S. F. Oliveira, N. Gnadt, I. Pacheco, A. V. Coelho, A. V. Xavier, M. Teixeira, C. M. Soares and I. A. Pereira, *JBIC, J. Biol. Inorg. Chem.*, 2005, **10**, 667–682.
140 S. Anantharaj, S. R. Ede, K. Sakthikumar, K. Karthick, S. Mishra and S. Kundu, *ACS Catal.*, 2016, **6**, 8069–8097.
141 P. Knörzer, A. Silakov, C. E. Foster, F. A. Armstrong, W. Lubitz and T. Happe, *J. Biol. Chem.*, 2012, **287**, 1489–1499.
142 W. J. Shaw, *Catal. Rev.*, 2012, **54**, 489–550.
143 G. Caserta, S. Roy, M. Atta, V. Artero and M. Fontecave, *Curr. Opin. Chem. Biol.*, 2015, **25**, 36–47.
144 T. Abe, T. Yoshida, S. Tokita, F. Taguchi, H. Imaya and M. Kaneko, *J. Electroanal. Chem.*, 1996, **412**, 125–132.
145 T. Yoshida, K. Kamato, M. Tsukamoto, T. Iida, D. Schlettwein, D. Wöhrle and M. Kaneko, *J. Electroanal. Chem.*, 1995, **385**, 209–225.
146 M. Xu, C. Li, H. Ren, L. Ding, K. Xu and J. Geng, *J. Mol. Catal. A: Chem.*, 2014, **390**, 69–75.
147 S. Samanta, P. K. Das, S. Chatterjee and A. Dey, *J. Porphyrins Phthalocyanines*, 2015, **19**, 92–108.
148 R. Cao, R. Thapa, H. Kim, X. Xu, M. G. Kim and Q. Li, *Nat. Commun.*, 2013, **4**, 2076.
149 D. Behar, T. Dhanasekaran, P. Neta, C. M. Hosten, D. Ejeh, P. Hambright and E. Fujita, *J. Phys. Chem. A*, 1998, **102**, 2870–2877.
150 A. J. Esswein and D. G. Nocera, *Chem. Rev.*, 2007, **107**, 4022–4047.
151 A. J. Morris, G. J. Meyer and E. Fujita, *Acc. Chem. Res.*, 2009, **42**, 1983–1994.
152 C. Costentin, S. Drouet, M. Robert and J. M. Savéant, *Science*, 2012, **338**, 90–94.
153 G. J. Samuels and T. J. Meyer, *J. Am. Chem. Soc.*, 1981, **103**, 307–312.
154 J. M. Calvert and T. J. Meyer, *Inorg. Chem.*, 1982, **21**, 3978–3989.
155 H. J. Son, C. Prasittichai, J. E. Mondloch, L. Luo, J. Wu, D. W. Kim, O. K. Farha and J. T. Hupp, *J. Am. Chem. Soc.*, 2013, **135**, 11529–11532.
156 K. Hanson, M. D. Losego, B. Kalanyan, G. N. Parsons and T. J. Meyer, *Nano Lett.*, 2013, **13**, 4802–4809.
157 K. Hanson, M. D. Losego, B. Kalanyan, D. L. Ashford, G. N. Parsons and T. J. Meyer, *Chem. Mater.*, 2013, **25**, 3–5.
158 Y. W. Chen, J. D. Prange, S. Dühnen, Y. Park, M. Gunji, C. E. Chidsey and P. C. McIntyre, *Nat. Mater.*, 2011, **10**, 539–544.
159 S. Hu, N. S. Lewis, J. W. Ager, J. Yang, J. R. McKone and N. C. Strandwitz, *J. Phys. Chem. C*, 2015, **119**, 24201–24228.
160 G. F. Moore, J. D. Blakemore, R. L. Milot, J. F. Hull, H. E. Song, L. Cai, C. A. Schmuttenmaer, R. H. Crabtree and G. W. Brudvig, *Energy Environ. Sci.*, 2011, **4**, 2389–2392.
161 Z. Yu, F. Li and L. Sun, *Energy Environ. Sci.*, 2015, **8**, 760–775.
162 R. J. Kamire, K. L. Materna, W. L. Hoffeditz, B. T. Phelan, J. M. Thomsen, O. K. Farha, J. T. Hupp, G. W. Brudvig and M. R. Wasielewski, *J. Phys. Chem. C*, 2017, **121**, 3752–3764.
163 D. L. Ashford, A. M. Lapides, A. K. Vannucci, K. Hanson, D. A. Torelli, D. P. Harrison, J. L. Templeton and T. J. Meyer, *J. Am. Chem. Soc.*, 2014, **136**, 6578–6581.
164 N. Ayres, *Polym. Chem.*, 2010, **1**, 769–777.
165 T. Chen, I. Amin and R. Jordan, *Chem. Soc. Rev.*, 2012, **41**, 3280–3296.
166 M. G. Moffitt, *J. Phys. Chem. Lett.*, 2013, **4**, 3654–3666.
167 M. Kim, S. Schmitt, J. Choi, J. Krutty and P. Gopalan, *Polymers*, 2015, **7**, 1346–1378.